A NEW APPROACH OF ZONAL HYBRID RANS-LES BASED ON A TWO-EQUATION $k-\varepsilon$ MODEL

L. Davidson

Department of Applied Mechanics, Chalmers University of Technology
SE-412 96 Gothenburg, Sweden

lada@chalmers.se

Abstract

A new zonal hybrid RANS-LES model is presented and evaluated in fully developed channel flow. The PANS model is used in both the URANS region (near the wall) and the LES region (away from the wall). In the URANS region, f_k is set to one and, in the LES region, f_k is set to a constant value (the baseline value is $f_k = 0.4$). The interface between the two regions is defined along a prescribed grid line. It is found that the new model gives good results for a large span of Reynolds numbers ($4\,000 \leq Re_\tau \leq 32\,000$). Three different grids are used in the wall-parallel planes, 32^2, 64^2 and 128^2, and – contrary to SGS models which use the filter as a turbulent lengthscale – the model yields virtually grid-independent results. In the LES region it is found that both the k equation and the ε equations are in local equilibrium. This is possible because there is a stronger correlation between P_k, ε and k^{-1} than between ε^2 and k^{-1} in the ε equation, compensating for the difference in C_1 and C_2^*.

1 Introduction

Wall-bounded Large Eddy Simulation (LES) is affordable only at low Reynolds number. At high Reynolds number, the LES must be combined with a URANS treatment of the near-wall flow region. There are different methods for bridging this problem such as Detached Eddy Simulation (DES) (Spalart; 2000; Spalart et al.; 1997) hybrid LES/RANS (Davidson and Peng; 2003a) and Scale-Adapted Simulations (SAS) (Menter and Egorov; 2010) (for a review, see Fröhlich and von Terzi (2008)). These models take the SGS length scale from the cell size (in SAS, the cell size is used as a limiter).

The partially averaged Navier-Stokes (PANS) model, proposed by Girimaji (2006), can be used to simulate turbulent flows either as a RANS, LES or DNS. An extension of PANS, based on a four-equation $k-\varepsilon-\zeta-f$ model, was recently proposed Basara et al. (2011). A near-wall low-Reynolds number capability was added to PANS so that the equations can be integrated all the way up to the wall (Ma et al.; 2011). In that work, it was furthermore shown that the PANS model is a good SGS model for wall-resolved LES at low Reynolds numbers. It was found that a constant value of $f_k = 0.4$ was appropriate (f_k is the ratio of modeled to total turbulent kinetic energy). In the present work, the PANS model is used as a zonal hybrid LES/RANS model to simulate wall-bounded flow at high Reynolds number. $f_k = 1$ in the near-wall region, and $f_k < 1$ in the LES region (a baseline value of 0.4 is used).

2 Equations

Mean flow equations

The momentum equations with an added turbulent viscosity reads

$$\frac{D\bar{u}_i}{Dt} = \delta_{1i} - \frac{1}{\rho}\frac{\partial \bar{p}}{\partial x_i} + \frac{\partial}{\partial x_j}\left((\nu+\nu_t)\frac{\partial \bar{u}_i}{\partial x_j}\right) \quad (1)$$

where D/Dt denotes the material derivative and the first term on the right side is the driving pressure gradient in the streamwise direction.

The PANS LRN $k-\varepsilon$ turbulence model

The low-Reynolds number partially averaged Navier-Stokes (LRN PANS) turbulence model reads (Ma et al.; 2011)

$$\begin{aligned}
\frac{Dk}{Dt} &= \frac{\partial}{\partial x_j}\left[\left(\nu+\frac{\nu_t}{\sigma_{ku}}\right)\frac{\partial k}{\partial x_j}\right] + (P_k - \varepsilon) \\
\frac{D\varepsilon}{Dt} &= \frac{\partial}{\partial x_j}\left[\left(\nu+\frac{\nu_t}{\sigma_{\varepsilon u}}\right)\frac{\partial \varepsilon}{\partial x_j}\right] + C_{\varepsilon 1}P_k\frac{\varepsilon}{k} - C_{\varepsilon 2}^*\frac{\varepsilon^2}{k} \\
\nu_t &= C_\mu\frac{k^2}{\varepsilon}, C_{\varepsilon 2}^* = C_{\varepsilon 1} + \frac{f_k}{f_\varepsilon}(C_{\varepsilon 2}f_2 - C_{\varepsilon 1}) \\
\sigma_{ku} &\equiv \sigma_k\frac{f_k^2}{f_\varepsilon}, \sigma_{\varepsilon u} \equiv \sigma_\varepsilon\frac{f_k^2}{f_\varepsilon}, \sigma_k = 1.4, \sigma_\varepsilon = 1.4 \quad (2) \\
C_{\varepsilon 1} &= 1.5, C_{\varepsilon 2} = 1.9, C_\mu = 0.09, f_\varepsilon = 1
\end{aligned}$$

In the baseline model, $f_k = 0.4$. The range of $0.2 < f_k < 0.6$ is evaluated.

The key element in the present use of the PANS model is that the $C_{\varepsilon 2}^*$ coefficient includes f_k. When f_k in the $C_{\varepsilon 2}^*$ coefficient is equal to one, the model acts as a standard $k-\varepsilon$ model. When f_k is decreased to, say,

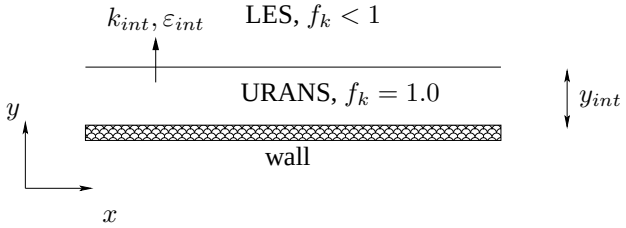

Figure 1: The URANS and the LES regions.

0.4, the destruction term is decreased, which increases ε. This reduces the modelled turbulent kinetic energy, k, and the turbulent viscosity and the model switches to an SGS (subgrid-scale) model.

The interface conditions.

The interface plane separates the URANS region near the wall and the LES region in the outer region. In the former region, the turbulent viscosity, ν_t, should be a RANS viscosity and in the latter region it should be an SGS viscosity. Hence ν_t must decrease rapidly when going from the URANS region to the LES region. This is achieved by setting the usual convection and diffusion fluxes of k at the interface to zero. New fluxes are introduced in which the interface condition is set to $k_{int} = f_k k_{RANS}$, where k_{RANS} is the k value in the cell located in the URANS region adjacent to the interface. Unless otherwise stated, no modification is made for the convection and diffusion of ε across the interface. The implementation is presented in some detail below. We write the discretized equation in the y direction (see Fig. 1) as (Versteegh and Malalasekera; 1995)

$$a_P k_P = a_N k_N + a_S k_S + S_U, a_P = a_S + a_N - S_P$$

where a_S and a_N are related to the convection and diffusion through the south and north face, respectively, and S_U and $S_P k_P$ include the production and the dissipation term, respectively. For a cell in the LES region adjacent to the interface (cell P), a_S is set to zero, cutting off the usual convection and diffusion fluxes. New fluxes are included in additional source terms as

$$\begin{aligned} S_U &= (C_s + D_s) f_k k_S, \quad S_P = -(C_s + D_s) \\ C_s &= \max\left(\bar{v}_s A_s, 0\right), \quad D_s = \frac{\mu_{tot} A_s}{\Delta y} \end{aligned} \tag{3}$$

where C_s and D_s denote convection (first-order upwind) and diffusion, respectively, through the south face, and A_s is the south area of the cell.

3 Numerical Method

An incompressible, finite volume code is used (Davidson and Peng; 2003b). The numerical procedure is based on an implicit, fractional step technique with a multigrid pressure Poisson solver and a non-staggered grid arrangement. For the momentum equations, central differencing is used in space and the Crank-Nicolson scheme is used in the time domain.

The first-order hybrid central/upwind scheme in space and the Crank-Nicolson scheme for time discretization are used in solving for the k and ε equations in the entire domain.

4 Results

Fully developed channel flow is computed for Reynolds numbers $Re_\tau = u_\tau \delta/\nu = 4\,000$, $8\,000$, $16\,000$ and $32\,000$. The baseline mesh has 64×64 cells in the streamwise (x) and spanwise (z) directions, respectively. The size of the domain is $x_{max} = 3.2$, $y_{max} = 2$ and $z_{max} = 1.6$ ($\delta = u_\tau = 1$). A simulation with twice as large domain in the $x - z$ plane ($x_{max} = 6.4$ and $z_{max} = 3.2$) with 128×128 cells was also made for $Re_\tau = 4\,000$, and identical results were obtained as for the smaller domain. The number of cells in the y direction varies between 80 and 128 cells depending on the Reynolds number, see Table 1. The baseline position for the interface is at $y^+ \simeq 500$ for all grids unless otherwise stated.

Re_τ	Δy^+	Δx^+	Δz^+	N_y
4 000	$2.2 - 520$	200	100	80
8 000	$1.5 - 1\,050$	400	200	96
16 000	$0.3 - 2\,100$	800	400	128
32 000	$0.6 - 4\,200$	1 600	800	128

Table 1: Grids. $f_y = 1.15$ (stretching).

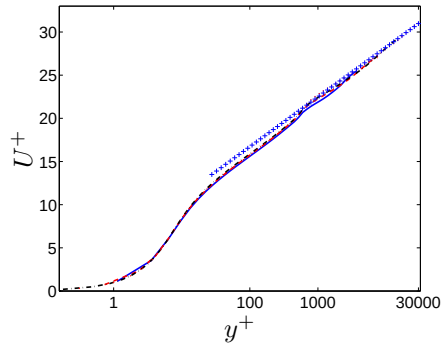

(a) Velocity

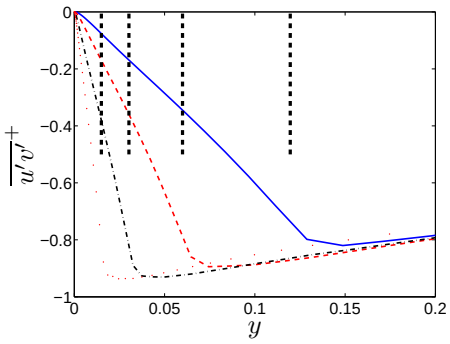

(b) Resolved shear stress

Figure 2: Velocity and resolved shear stress. $(N_x \times N_z) = (64 \times 64)$ ——: $Re_\tau = 4\,000$; - - -: $Re_\tau = 8\,000$; - - -: $Re_\tau = 16\,000$; ····: $Re_\tau = 32\,000$. Vertical thick dashed lines show the interface line between the URANS and the LES region.

The velocity profiles and the resolved shear stresses are presented in Fig. 2. As can be seen, the predicted velocity profiles are in good agreement with the log-law. Figure 2b presents the resolved shear stresses. The interface is shown by thick dashed vertical lines; it moves towards the wall for increasing Reynolds number since it is located at $y^+ \simeq 500$ for all Reynolds numbers.

Figures 3 and 4 present the velocity and shear stress profiles on coarse meshes (half as fine in x and z) and fine meshes (twice as fine in x and z), respectively. The results are almost the same as on the baseline mesh (the velocity profile on the coarse mesh for the highest Reynolds number is slightly worse).

The baseline value of the position of the interface is $y^+ \simeq 500$. Figure 5 presents the sensitivity to the posi-

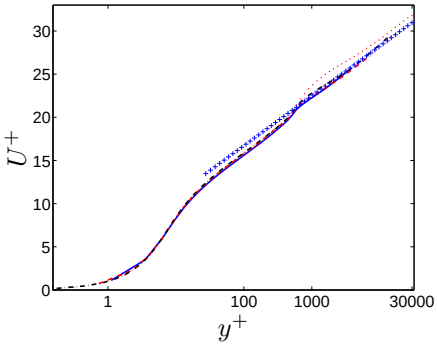

(a) Velocity

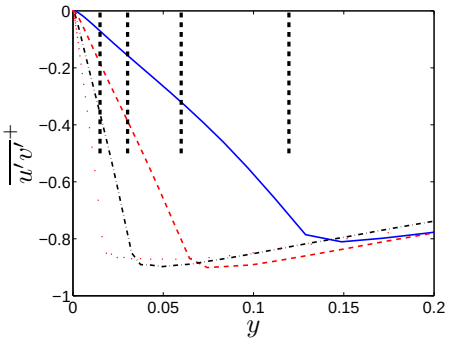

(b) Resolved shear stress

Figure 3: Velocity and resolved shear stress. $(N_x \times N_z) = (32 \times 32)$. For legend, see Fig. 2.

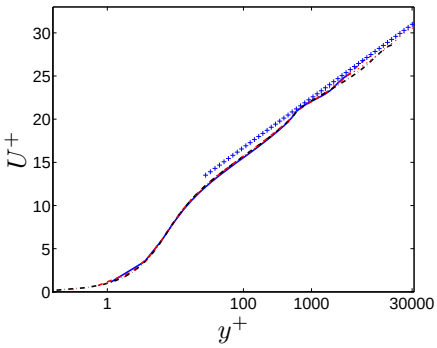

(a) Velocity

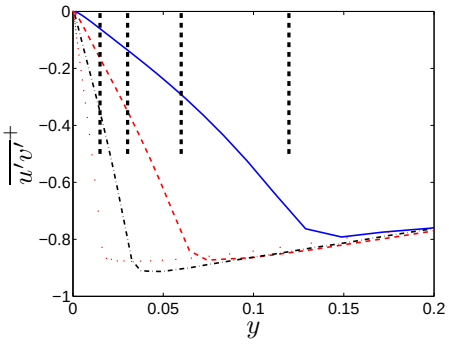

(b) Resolved shear stress

Figure 4: Velocity and resolved shear stress. $(N_x \times N_z) = (128 \times 128)$. For legend, see Fig. 2.

tion of the interface. The peak in the viscosity profiles is located approximately in the middle of the URANS region. It can be seen that, as the interface is moved closer to the wall, the peak of the turbulent viscosity

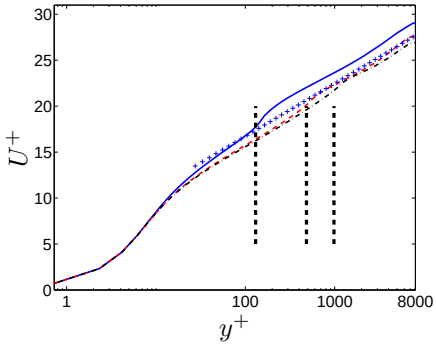

(a) Velocity

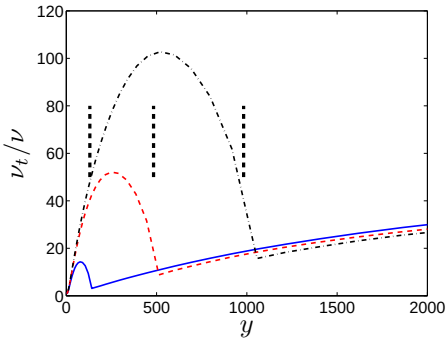

(b) Turbulent viscosity

Figure 5: Velocity and turbulent viscosity. $Re_\tau = 8000$. Interface location at ——: $y^+ = 130$ - - -: $y^+ = 500$ - · -: $y^+ = 980$.

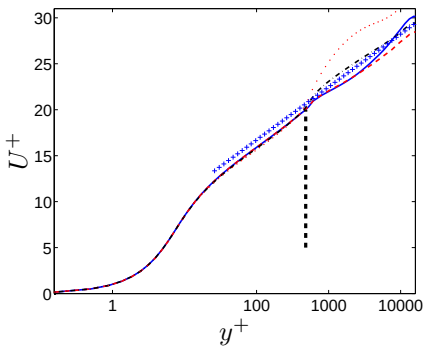

(a) Velocity

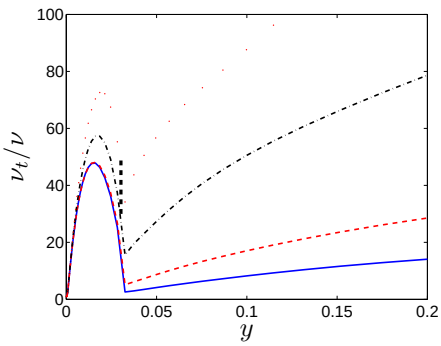

(b) Turbulent viscosity

Figure 6: Velocity and turbulent viscosity. $Re_\tau = 8000$. Influence of f_k. ——: $f_k = 0.2$ - - -: $f_k = 0.3$ - · -: $f_k = 0.5$ ····: $f_k = 0.6$

gets smaller. At the innermost location ($y^+ = 130$), the velocity profile is poorly predicted, but, if the loca-

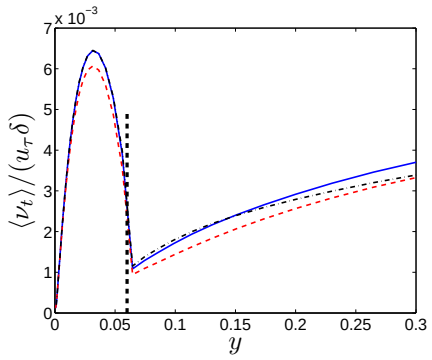

Figure 7: Turbulent viscosity. $Re_\tau = 8000$. ——: $(N_x \times N_z) = (64 \times 64)$; - - -: $(N_x \times N_z) = (32 \times 32)$; - · -: $(N_x \times N_z) = (128 \times 128)$.

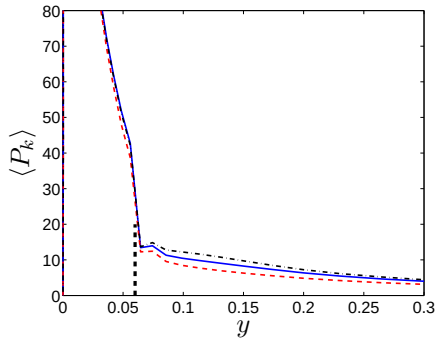

Figure 8: Production term, P_k. $Re_\tau = 8000$. ——: $(N_x \times N_z) = (64 \times 64)$; - - -: $(N_x \times N_z) = (32 \times 32)$; - · -: $(N_x \times N_z) = (128 \times 128)$.

tion is in the region of $500 < y^+ < 1000$, the velocity profile is well predicted.

Figure 6 presents the effect of f_k on the predicted velocity and turbulent viscosity. The turbulent viscosity increases, as expected, for increasing values of f_k. The velocity profile is very well predicted with $f_k = 0.5$ and rather well with $f_k = 0.3$. For $f_k = 0.6$ the velocity profile is poorly predicted because of the large turbulent viscosity which approaches RANS values in the outer region.

The turbulent viscosity profiles are shown in Fig. 7 for three different resolutions in the $x - z$ plane. It is interesting to note that the turbulent viscosity is not affected by the grid resolution. Hence, the model yields *grid independent* results. Note that the ratio of the filter width, $\Delta = (\Delta V)^{1/3}$, for the fine grid (128×128) to that on the coarse (32×32) grid is $16^{1/3} \simeq 2.5$. Hence, an SGS model based on Δ would give a 2.5 larger viscosity on the coarse mesh than on the fine mesh. In hump flow simulations carried out by Davidson and Peng (2011) using PANS, it was also found that a grid refinement (doubling the number of cells in the spanwise direction) gave no reduction in the turbulent viscosity.

It can be seen that the turbulent viscosity (Fig. 7) is sharply reduced when moving across the interface from the URANS region to the LES region. This is achieved by the modified interface convection and diffusion fluxes in the k equation, see Eq. 3.

It was shown in Fig. 7 that the turbulent viscosity is independent of the grid. The production term, $\langle P_k \rangle = \langle \varepsilon_{SGS} \rangle$, also stays constant when the grid is refined or coarsened, see Fig. 8. This is correct since the amount of energy fed into the turbulence energy spectrum should be independent upon the grid resolution. As expected, the k equation is in local equilibrium, i.e. $\langle P_k \rangle = \langle \varepsilon \rangle$, see Fig. 9a. Interestingly, the time-averaged production and dissipation terms in the ε equation are also in balance, see Fig. 9b. If both the k and the ε equations are in local equilibrium, we have (see Eq. 2)

$$P_k - \varepsilon = 0, \quad \frac{\varepsilon}{k}(C_1 P_k - C_2^* \varepsilon) = 0 \qquad (4)$$

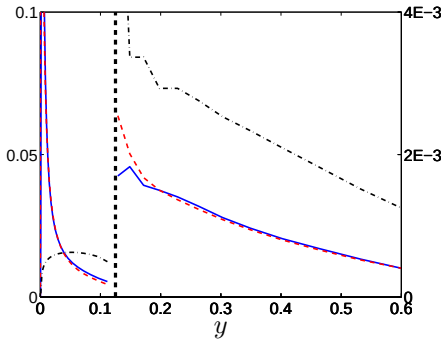

(a) ——: $\langle P_k \rangle^+$; - - -: $\langle \varepsilon \rangle^+$; - · -: $\langle C^k_{rms} \rangle^+$

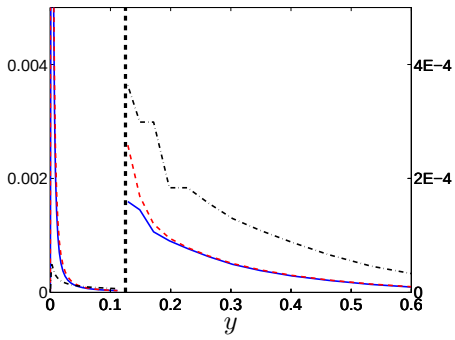

(b) ——: $\langle C_{\varepsilon 1} P_k/\varepsilon \rangle^+$; - - -: $\langle C_{\varepsilon 2} \varepsilon^2/k \rangle^+$; - · -: $\langle C^\varepsilon_{rms} \rangle^+$

Figure 9: Production, destruction and RMS of convection terms in the k and ε equations. Inner scaling. Left vertical axes: inner (URANS) region; right vertical axes: outer (LES) region. $Re_\tau = 4000$. $(N_x \times N_z) = (64 \times 64)$.

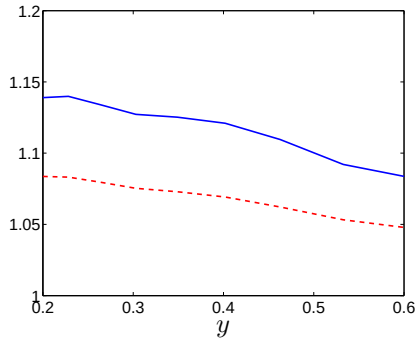

Figure 10: Production and destruction terms in the k and ε equations. ——: $\dfrac{\langle \varepsilon P_k/k \rangle}{\langle \varepsilon \rangle \langle P_k \rangle / \langle k \rangle}$ - - -: $\dfrac{\langle \varepsilon^2/k \rangle}{\langle \varepsilon^2 \rangle / \langle k \rangle}$

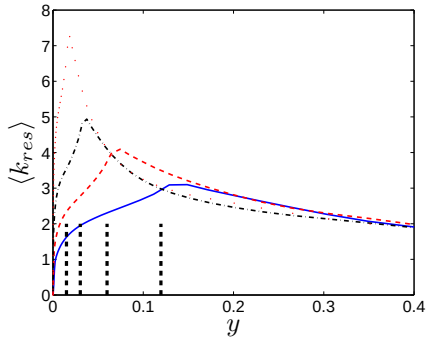

(a) Resolved, k_{res}

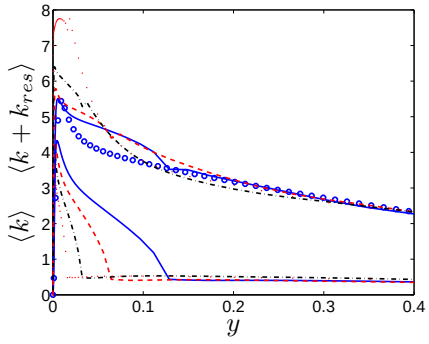

(b) Modelled, k (lower curves) and total, $k + k_{res}$ (upper curves)

Figure 11: Turbulent kinetic energies. $(N_x \times N_z) = (64 \times 64)$. For legend, see Fig. 2. $\circ$: DNS at $Re_\tau = 2000$ (Hoyas and Jiménez; 2006a,b)

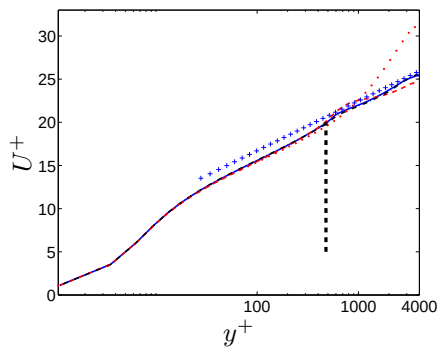

(a) Velocity

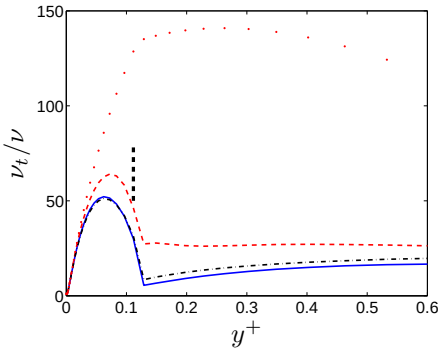

(b) Turbulent viscosity

Figure 12: Velocity and turbulent viscosity. $Re_\tau = 4000$. $(N_x \times N_z) = (64 \times 64)$. Influence of C_s in Eq. 8. ——: $C_s = 0.1$; - - -: $C_s = 0.5$; - - -: no interface condition on ε; ····: no interface condition on ε or k.

They cannot both be satisfied since $C_1 \neq C_2^*$. It is found that the instantaneous convective terms in the k and the ε equations – although their time average is zero – are of the same order as the production and dissipation terms, see Fig. 9. Hence, instantaneously, the production, destruction and convection terms are the important terms in the k and the ε equations.

But one question remains: how can the *time-averaged* production and destruction terms in both the k and ε equations (Eq. 4) be in balance? The reason is that although

$$C_1 \frac{\langle \varepsilon \rangle}{\langle k \rangle} \langle P_k \rangle \neq C_2^* \frac{\langle \varepsilon \rangle^2}{\langle k \rangle} \tag{5}$$

(because $\langle P_k \rangle = \langle \varepsilon \rangle$), Fig. 8 shows that

$$C_1 \left\langle \frac{\varepsilon}{k} P_k \right\rangle = C_2^* \left\langle \frac{\varepsilon^2}{k} \right\rangle \tag{6}$$

It is a general feature of any two turbulent quantities, $A = \langle A \rangle + A'$ and $B = \langle B \rangle + B'$, that $\langle AB \rangle \neq \langle A \rangle \langle B \rangle$. In the case of Eq. 6, the correlation between P_k, ε and k^{-1} is stronger than that between ε^2 and k^{-1}, as shown in Fig. 10.

It was mentioned above that the supply of turbulent kinetic energy from the mean flow to large, energy-containing eddies in the turbulence energy spectrum should be grid independent. As a consequence, the SGS dissipation, $\varepsilon_{SGS} = P_k$, at the small scales should also be grid independent. The SGS dissipation is formulated as $\varepsilon_{SGS} = 2\langle \nu_t \bar{s}_{ij} \bar{s}_{ij} \rangle$. It was shown in Davidson (2009) that the time-averaged strain $\langle \bar{s}_{ij} \rangle \langle \bar{s}_{ij} \rangle$ is negligible compared to the fluctuating one, i.e. $\langle \bar{s}'_{ij} \bar{s}'_{ij} \rangle \gg \langle \bar{s}_{ij} \rangle \langle \bar{s}_{ij} \rangle$, which means that the SGS dissipation can be written as

$$\varepsilon_{SGS} = 2\langle \nu_t \bar{s}_{ij} \bar{s}_{ij} \rangle \simeq 2\langle \nu_t \bar{s}'_{ij} \bar{s}'_{ij} \rangle \tag{7}$$

Zero equation SGS models based on the cell size (e.g. the Smagorinsky model) compute the SGS viscosity as the product of the square of the filter size, Δ^2, and the magnitude of the strain rate, $|\bar{s}|$. In order to satisfy the requirement that ε_{SGS} is grid independent, the strain rate must compensate (i.e. increase) for the decrease in Δ when the grid is refined. To be able to increase $\bar{s}_{ij}$ when the grid is refined, the SGS dissipation must take place at larger wavenumbers compared to the coarse grid. This put high requirements on the accuracy of the discretization and is probably one reason why the SGS models based on the filter width are so sensitive to grid refinement. It was shown in Davidson (2009, 2010) that the SGS dissipation did to some extent take place at higher wavenumber when the grid was refined in channel flow and diffuser flow, but the effect was not sufficient to compensate for decrease in filter width. The present model seems to much better in this respect. A drawback of the present model may be that, as the grid is refined towards DNS, the modelled viscosity does not go to zero. On the other, this is rarely an issue in industrial applications.

Figure 11 shows how the modelled, resolved and total turbulent kinetic energy vary for different Reynolds numbers. It was shown in Yakhot et al.

(2010) that the turbulent kinetic energy should be independent of Reynolds number provided that $Re_{2h} > 10^5$ ($Re_\tau \gtrsim 2000$). As can be seen, this is well satisfied in the outer region ($y > 0.1$) where the total kinetic energies also agree nicely with DNS data. For the highest Reynolds number, the resolved kinetic energy is too large near the wall.

No special treatment was used for ε at the interface in the simulations presented above. Initially, simulations were made in which the convection and the diffusion were modified in the same way as for k, see Eq. 3. The ε value that was transported from the URANS region to the LES region was set from the Smagorinsky model in the same way as in embedded LES (Davidson and Peng; 2011)

$$\varepsilon_S = C_\mu^{3/4} k_S^{3/2} / \ell_{sgs}, \quad \ell_{sgs} = C_s \Delta \qquad (8)$$

where $\Delta = V^{1/3}$, and V is the volume of the cell adjacent to the interface. A value of $C_s = 0.07$ was found to be suitable for embedded LES. Figure 12 presents simulations using different values of C_s. The results achieved when using

- no interface condition on ε
- no interface condition on k, ε

are also included for reference. First, it can be noted that when using no interface condition on k, the turbulent viscosity in the LES region becomes much too large, and as a consequence the velocity profile is poorly predicted. Furthermore, a value of $C_s = 0.1$ give a good agreement with the log-law; a value of $C_s = 0.05$ gives almost identical results (not shown). Theses small C_s values succeed in strongly reducing the turbulent viscosity in the LES region adjacent to the interface. When making these tests it was realized that the best and most accurate treatment of ε at the interface is to do nothing at all. It turns out that computing C_s from Eq. 8 in the post-processing using data for which no interface condition on ε was used gives a value of $C_s = 0.11$.

5 Conclusions

A new approach for using PANS as a zonal hybrid RANS-LES model has been presented. It has been evaluated for channel flow at different Reynolds numbers ($4\,000 \leq Re_\tau \leq 32\,000$) and gives good agreement with the log-law. Furthermore, it was found that the model gives virtually grid-independent results when refining the grid in the wall-parallel planes ($N_x \times N_z = 32 \times 32$, 64×64 and 128×128). The turbulent viscosities obtained on these three grid are nearly the same. An SGS model using the cell size as a turbulent length scale would give a $16^{1/3} \simeq 2.5$ larger turbulent lengthscale on the finest mesh compared to the coarsest mesh.

Acknowledgments

The financial support of SNIC (the Swedish National Infrastructure for Computing) for computer time at C3SE (Chalmers Center for Computational Science and Engineering) is gratefully acknowledged. This project was financed by the EU project ATAAC (Advanced Turbulence Simulation for Aerodynamic Application Challenges), Grant Agreement No. 233710. `http://cfd.mace.manchester.ac.uk /ATAAC/WebHome`

References

Basara, B., Krajnović, S., Girimaji, S. and Pavlović, Z. (2011). Near-wall formulation of the Partially Averaged Navier Stokes turbulence model, *AIAA Journal* **49**(12): 2627–2636.

Davidson, L. (2009). Large eddy simulations: how to evaluate resolution, *International Journal of Heat and Fluid Flow* **30**(5): 1016–1025.

Davidson, L. (2010). How to estimate the resolution of an LES of recirculating flow, *in* M. V. Salvetti, B. Geurts, J. Meyers and P. Sagaut (eds), *ERCOFTAC*, Vol. 16 of *Quality and Reliability of Large-Eddy Simulations II*, Springer, pp. 269–286.

Davidson, L. and Peng, S.-H. (2003a). Hybrid LES-RANS: A one-equation SGS model combined with a $k - \omega$ for predicting recirculating flows, *International Journal for Numerical Methods in Fluids* **43**: 1003–1018.

Davidson, L. and Peng, S.-H. (2003b). Hybrid LES-RANS: A one-equation SGS model combined with a $k-\omega$ model for predicting recirculating flows, *International Journal for Numerical Methods in Fluids* **43**: 1003–1018.

Davidson, L. and Peng, S.-H. (2011). Emdedded LES with PANS, *6th AIAA Theoretical Fluid Mechanics Conference, AIAA paper 2011-3108*, 27-30 June, Honolulu, Hawaii.

Fröhlich, J. and von Terzi, D. (2008). Hybrid LES/RANS methods for the simulation of turbulent flows, *Progress in Aerospace* **44**(5): 349–377.

Girimaji, S. (2006). Partially-Averaged Navier-Stokes model for turbulence: A Reynolds-averaged Navier-Stokes to direct numerical simulation bridging method, *Journal of Fluids Engineering* **73**(2): 413–421.

Hoyas, S. and Jiménez, J. (2006a). http://torroja.dmt.upm.es/ftp/channels/data/statistics/.

Hoyas, S. and Jiménez, J. (2006b). Scaling of the velocity fluctuations in turbulent channels up to $Re_\tau = 2003$, *Physics of Fluids A* **18**(011702).

Ma, J., Peng, S.-H., Davidson, L. and Wang, F. (2011). A low Reynolds number variant of Partially-Averaged Navier-Stokes model for turbulence, *International Journal of Heat and Fluid Flow* **32**: 652–669.

Menter, F. and Egorov, Y. (2010). The scale adaptive simulation method for unsteady turbulent flow predictions. Part 1: Theory and description, *Flow, Turbulence and Combustion* **85**: 113–138.

Spalart, P. (2000). Strategies for turbulence modelling and simulations, *International Journal of Heat and Fluid Flow* **21**: 252–263.

Spalart, P., Jou, W.-H., Strelets, M. and Allmaras, S. (1997). Comments on the feasability of LES for wings and on a hybrid RANS/LES approach, *in* C. Liu and Z. Liu (eds), *Advances in LES/DNS, First Int. conf. on DNS/LES*, Greyden Press, Louisiana Tech University.

Versteegh, H. and Malalasekera, W. (1995). *An Introduction to Computational Fluid Dynamics - The Finite Volume Method*, Longman Scientific & Technical, Harlow, England.

Yakhot, V., Bailey, S. and Smits, A. (2010). Scaling of global properties of turbulence and skin friction in pipe and channel flows, *Journal of Fluid Mechanics* **652**: 65–73.